

Temporal–Spatial Dew Formation Potential in Jordan – Identification of Dew Formation Zones

Nahid Atashi^{1,2}, Tareq Hussein^{1,3*}

¹ University of Helsinki (UH), Faculty of Science, Institute for Atmospheric and Earth System Research (INAR/Physics), Helsinki, Finland

² Faculty of Geographical Science and Planning, University of Isfahan, Isfahan, Iran

³ The University of Jordan, School of Science, Department of Physics, Amman, Jordan

Received 29th May 2021; Accepted 29th January 2022

Abstract

Jordan is the fourth country in the world suffering from freshwater shortages. Therefore, this research aims to investigate the dew formation potential as an alternative source of water in Jordan. We performed gridded model simulations to estimate the dew yield during 1979–2018. We also utilized cluster analysis to identify the dew formation zones in Jordan. Our investigation revealed that dew can occur almost everywhere in Jordan during the winter (~75 days). As expected, summer is the driest season with the least number of dew days (~37 days). According to the cluster analysis, we distinguished three dew formation zones, which were closely related to the climate zones: Dew zone A (eastern desert), Dew zone B (Jordan Valley), and Dew Zone C (central heights Plateau). Zone A receives the least dew formation potential (on average 0.05 L/m²/day), which mainly occurs during the winter, and Zone B receives the highest dew formation potential (on average 0.15 L/m²/day), which occurs throughout the year. The average yearly dew yield in dew zone A, B, and C was about 18, 55, and 28 L/m². The outcomes of this study are ought to be useful for managing and planning local feasibility studies for dew harvesting and a better understanding of the feedback processes between the water cycle and climate change in Jordan.

© 2022 Jordan Journal of Earth and Environmental Sciences. All rights reserved

Keywords: Dew formation, heat-transfer balance, cluster analysis, long-term analysis.

1. Introduction

Jordan has been one of the countries that suffered from the climate change impacts on water resources and supplies. This disruption imposed socio-economic consequences that might take many years to recover. Like many other countries, Jordanians will suffer from freshwater shortage by the year 2025 (Lindblom et al., 2006). Accordingly, awareness, international agreements, and national strategies must be built up to wisely manage and restore water resources in Jordan (Lekouch et al., 2011). For example, technological advancement (e.g. water desalination, enhanced rain programs, dew, and fog harvesting) plays an important role in decreasing the effects of climate change on water resources (Khalil et al., 2016; MaestreValero et al., 2011; Mileta et al., 2019; Agam et al., 2006; Kidron et al., 2002; Nikolayev et al., 1996; Nilsson et al., 1994; Rajvanshi, 1981; Jumikis, 1965; Hamed et al., 2010).

Water is continuously re-circulated and transported between oceans, land, and the atmosphere forming the so-called Earth's hydrologic cycle. Besides, vertical convection of water vapor and cloud formation, water vapor might transport nearby the Earth's surface and end up forming fog, smog, and mist as well as the condensation on cooled surfaces (i.e., dew formation). In fact, dew and fog formation is a very complex phenomenon that has been understood as a two-step process (Beysens et al., 2003, 2005 and 2006a; Beysens 1995 and 2006; Muselli et al., 2002; Raman et al., 1973): (1) formation of droplets on obstacles (particle, surface, etc.) via nucleation of water vapor and (2) droplet

growth due to condensation of water vapor.

The amount and quality of harvested dew water have been given growing attention (Alnaser et al. 2006; Beysens et al., 2006b and 2007; Galek et al., 2012 and 2015; Lekouch et al., 2010; Odeh et al 2017; Polkowska et al., 2008). Several groups have developed different methods and tools to harvest dew in different environments (Odeh et al., 2017; Clus et al., 2008; Muselli, et al., 2009; Richards, 2019; Sharan et al., 2007 and 2019; Ye et al., 2007; Vuollekoski et al., 2015; Tomaszkiwicz et al., 2015). The most common experimental methods included passive condensers, radiative cooling, roofs (made of different materials, and surfaces made of a material that enhances the yield of dew. However, sustainable and long-term experimental studies about dew formation seem to be almost impossible. Therefore, the potential of dew formation has been investigated using model simulation. The simplest and most applicable models are those based on the semi-empirical approaches to implementing heat-mass transfer and energy balance (Nikolayev et al., 1996 2001; Beysens et al., 2003 and 2005; Vuollekoski et al., 2015; Tomaszkiwicz et al., 2015 and 2016; Monteith, 1957; Beysens, 2016; Gandhisam et al., 2005; Pedro et al., 1981; Nilsson, 1996; Jacobs et al., 2008; Jorge Ernesto et al., 2016). In Jordan, there have been only three investigations about dew water (Jiries, 2001; Odeh et al., 2017; Atashi et al., 2020, Al-Shuaiibi, 2021). The first one reported some elemental and ion concentrations in dew water (Jiries, 2001). In the second one, Odeh et al.

* Corresponding author e-mail: t.hussein@ju.edu.jo

(2017) collected 15 samples of dew water on a substrate (during March–July 2015) in an urban area in Amman and reported the collected amount and quality by applying chemical and physical analysis. The third investigation included long-term model simulations for dew potential at ten selected locations reflecting the different climate zones in Jordan (Atashi et al. 2020). The most recent research on dew water harvesting quantity and quality was conducted at an urban site in Jordan (Al-Shuaibi R. 2021). However, dew formation zones have never been assessed theoretically in Jordan.

In this study, we performed gridded model simulations to estimate the dew yield during 1979–2018 aiming at distinguishing the dew formation zones in Jordan. The model simulations were made by adapting the global model, which was developed by Vuollekoski et al. (2015), to accommodate the environmental conditions in different environments in Jordan. The outcomes of this study are ought to be useful for managing and planning local feasibility studies for dew harvesting and a better understanding of the feedback processes between the water cycle and climate change in Jordan.

2. Data and Methods

2.1 An overview of the climate and water resources in Jordan

Jordan is a small country (29.4°–33° North and 35°–39.5° East, (~89,000 km², population ~11 million in 2021) with limited water sources and diverse habitats, ecosystems, and biota. The summer season (May–September) is hot-dry with a mean temperature of ~32 °C. The winter (November–March) is relatively cool with a mean temperature of ~13 °C and frequent showers and occasional snowfall in some elevated areas. Geographically, Jordan comprises a wide variety of topography that defines its climate spatial variation (Abdulla, 2020; Freiwan and Kadioglu, 2008): (1) semi-arid climate in the Jordan Valley with a hot dry summer, warm winter, and precipitation less than 200 mm/yr.; (2) arid climate in the Eastern Desert (also known as Badia) characterized by a sharp change in temperature between day and night and between summer and winter; and (3) Mediterranean climate on the Mountains Heights Plateau (including highlands above the Jordan Valley, mountains of the Dead Sea, Wadi Araba, and Ras Al-Naqab) with a hot-dry summer and cool-wet winter and two short transitional seasons. The Mountains Heights Plateau receives Jordan’s highest amounts of precipitation (more than 300 mm/year), which falls from October to May with the peak usually during winter (December–February).

Jordan is the fourth country in the world suffering from freshwater shortages (Hamdy et al., 1999; Hadadin, 2015). The available water per capita has declined considerably during the past century; it was about 3600 m³ in 1946 and it is expected to be as low as 100 m³ in 2025 (Hadadin, 2015). Jordan’s water demand was estimated to be about 940 MCM (63% agriculture, 32% domestic, and 5% industry) in 2007 and it increased to about 1600 MCM in 2010. The main sources of water include safe abstraction of groundwater, recycling wastewater, surface runoff water, and desalination. The annual mean water amount received in the form of

rainfall is about 8300 million cubic meters (MCM) (Hamdy et al., 1999).

2.2 Meteorological input data

The meteorological input data-base includes horizontal and vertical wind components (U10 and V10) at 2 m, surface roughness (z0), ambient temperature and dew point (Ta and DP) at 2 m, and short-wave and long-wave surface solar radiation (R_{sw} and R_{lw}). The input database was downloaded from the European Centre for Medium-Range Weather Forecast (ECMWF) Interim Reanalysis (ERA-Interim), which is a global atmospheric reanalysis that is available from 1 January 1979 to 31 August 2019 (Berrisford et al., 2011; Dee et al., 2011). ERA-Interim has a native resolution of 0.75° (approximately 80 km) and 60 vertical levels. In this study, we considered the time during 1979- 2018 and input data interpolated to a grid resolution of 0.25 (~ 30 km) over a domain covering all parts of Jordan. The ERA-Interim is differentiated into two main categories: analysis fields and forecast fields (i.e. instantaneous and accumulated forecast). The analysis fields were available every 6 h (00:00, 06:00, 12:00, and 18:00 UTC) and the forecast fields were available every 3 h; hence, they can be used to fill in the gaps between the analysis. In our case, U10, V10, Ta, and DP were obtained from both analysis (i.e. at 00:00, 06:00, 12:00, and 18:00 UTC) and instantaneous forecast fields (i.e. at 03:00, 09:00, 15:00, and 21:00 UTC) and obtained the short-wave and long-wave (R_{sw} and R_{lw}) surface radiation as accumulated forecast fields. In the ERA-Interim database, the horizontal wind components (U₁₀ and V₁₀) are provided at 10 m. Therefore, the wind speed at 2 meters was calculated by using a logarithmic wind profile as follows:

$$WS = \frac{\log\left(\frac{z+z_0}{z_0}\right)}{\log\left(\frac{10+z_0}{z_0}\right)} \sqrt{U_{10}^2 + V_{10}^2} \dots\dots\dots (1)$$

where z₀ (as instanton forecast parameter) is the surface roughness and U₁₀ and V₁₀ are the horizontal wind speed components at 10 m.

2.3 Dew formation model

A global dew formation model, which was developed by Vuollekoski et al. (2015), was downscaled to simulate the dew formation potential in Jordan (Figure 1). The substrate (i.e., condenser material) was assumed a horizontally aligned sheet (at 2 m height and thermally insulated from the ground) of a suitable material such as low-density polyethylene (LDPE) or polymethylmethacrylate (PMMA). The detailed model description is presented in Supplementary Material (which I didn’t see in the article). In brief, the model describes the water phase change based on mass and heat balance Equation:

$$\frac{dT_c}{dt} (C_c m_c + C_w m_w + C_i m_i) = P_{rad} + P_{cond} + P_{conv} + P_{lat} \dots (2)$$

where dT_c/dt is the change rate in the condenser temperature. C_c, C_w, and C_i are the specific heat capacity of condenser, water, and ice; respectively. Here, m_c, m_w, and m_i are mass of condenser, water, and ice; respectively. The right-hand side describes the heat exchange involved in the heat exchange processes: P_{rad} is the net radiation, P_{cond} is the conductive heat exchange between the condenser surface and the ground, P_{conv} is the convective heat exchange, and P_{lat} is the latent heat released by the condensation or desublimation

of water. The model reads all input data (described in section 2.2) for a given grid point and solves the mass and heat balance equations using a fourth-order Runge–Kutta algorithm with a 10 s time step. The output is the cumulative daily dew yield in mm/m². All terms in Equation (S1) are described in more detail in Tables S1 and S2 (see Appendix).

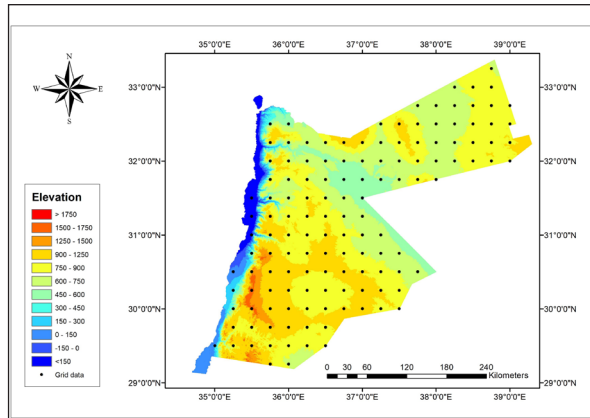


Figure 1. A map of Jordan illustrating the geographical topography and the domain of the grid points used in the model simulation.

Table 1. Dew formation zones and their climate features (i.e., mean (min-max) values for meteorological parameters (T, T_d, RH)) as well as statistical analysis for overall mean daily cumulative dew yield (i.e., std, 25, 50, 75th, and 99th percentile as daily max as well as yearly max dew yield).

	Zone A	Zone B	Zone C
T _{mean} [°C]	20 [19-2]	19 [12-26]	19 [12-26]
T _{d mean} [°C]	4 [3-6]	8 [5-11]	6 [4-8]
RH _{mean} [%]	42 [36-51]	57 [49-66]	49 [42-58]
Mean dew yield ± std [L/m ² /day]	0.05 ± 0.05	0.15 ± 0.03	0.08 ± 0.04
25% [L/m ²]	0.03	0.11	0.05
Median [L/m ²]	0.04	0.14	0.07
75% [L/m ²]	0.06	0.18	0.10
99% [L/m ²]	0.09	0.26	0.15
Mean [L/m ² /year]	18	55	28
Max [L/m ² /year]	26	66	36

2.4 Cluster Analysis

To identify the major dew formation zones in Jordan we applied Cluster Analysis (CA) to the long-term gridded model simulation. CA is an effective statistical technique that groups similar data points in the same group so that the objects in one group (called a cluster) are more similar to each other than in the other groups. There are two main clustering methods: hierarchical and non-hierarchical cluster analysis (Bunkers and Miller, 1996; Yim and Ramdeen, 2015). In this study, we used hierarchical agglomerative clustering which consists of four main steps (HAC, Nielsen, 2016).

1. calculating the distance measured between all entries (data points);
2. merging the two closest entries as a new cluster;
3. recalculating the distance between all entries;
4. repeat steps 2 and 3 until all entries are grouped into distinct groups (i.e., clusters). The details of the clustering method used in this study are described in the supplementary material (section S2). After calculating all the steps and visualizing the results, three clusters were chosen as an optimal number of clusters for Jordan.

3. Discussion and Results

3.1 Dew potential – Long-Term Simulation and Analysis

The model simulation results revealed that dew can occur almost everywhere in Jordan, even in the driest areas in the eastern part of the country. Figure 2 illustrates the frequency of seasonal dew occurrence as a fraction of days for any dew yield. The average frequency of dew was about 84% (~75 days) in wintertime (December–February, Figure 2a). After winter with the most frequency of dew days, spring (March–May) with 52% (~48 days, Figure 2b) and autumn (September–November) with 57% (~52 days, Figure 2d) have a modest frequency, respectively. As expected, summer (June–August) was the driest season with the least number of dew days in Jordan (40%, ~37 days, Figure 2c).

From the spatial point of view, in all cases, the dry eastern part has the minimum number of dew occurrences and the northwest part has the maximum. However, by limiting the dew occurrence analysis to dew yield > 0.1 L/m²/day, the frequency of dew days was reduced by about 30% (~25 days) in all seasons. Specifically, by considering this threshold (> 0.1 L/m²/day), the frequency of dew occurrence was about 15% (~14 days), 25% (~23 days), 32% (~29 days), and 57% (~51 days) and in the summer and spring, dew occurrence shrank to include mainly the western half of the country (Figure 1).

The seasonal mean of daily cumulative and also monthly dew yield is presented in Figure 3 and Figure 4; respectively. The seasonal mean of daily dew yield shows the same temporal and spatial pattern as the frequency map with the highest yields in winter (~0.13 L/m²/day, Figure 3a), and the lowest yields in summer (~0.03 L/m²/day, Figure 3c). These amounts for the transition months (i.e. autumn and spring) are about 0.07 and 0.05 L/m²/day. In spatial scale, the highest values are along with the highlands in the northwestern part of Jordan. The lowest values were belonging to the dry lands and deserts in the southeastern parts of the country.

A closer look at the spatial and temporal variation of dew yield can be seen from the monthly cumulative dew reflects the seasonal pattern (Figure 4). Based on the monthly analysis, dew can occur from October–March in almost whole areas with the highest yields in December and January whereas, from April–September except for the western areas (i.e. Jordan valley and coastal dead sea areas), dew almost vanishes in the rest parts of the country. High air temperature, low relative humidity, and long day duration in the warm seasons prevent dew condensation in most areas in Jordan, in turn, during the cold seasons by decreasing the air temperature and injecting moisture by the prevailing westerly winds, the difference between temperature and dew point temperature declines and the initial condition is provided for the formation of dew in the almost whole country.

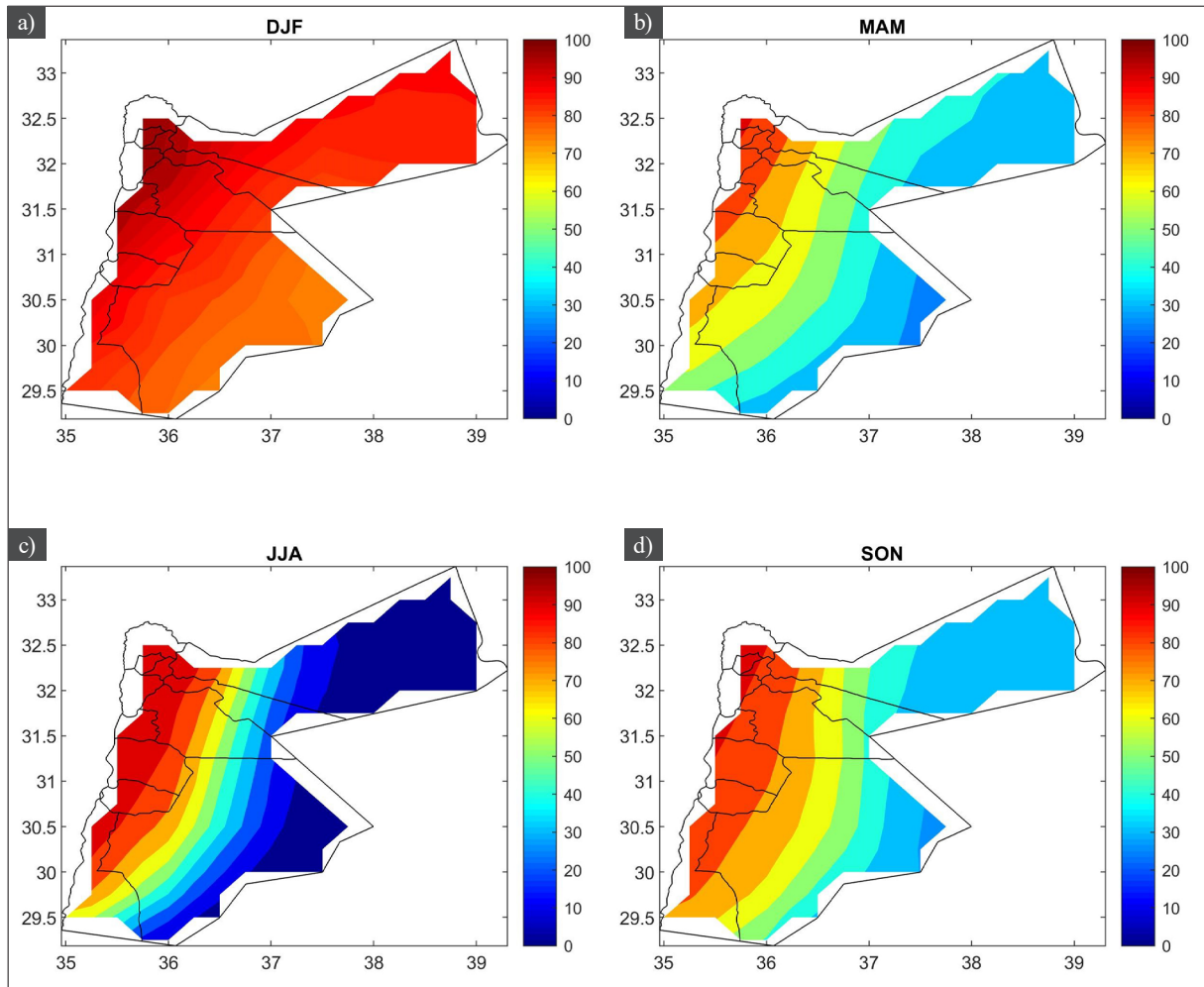


Figure 2. Frequency of dew occurrence as a fraction of days presented as an overall seasonal mean during 1979–2018. (a) winter (December, January, and February), (b) spring (March, April, and May), (c) summer (June, July, and August), and (d) autumn (September, October, and November).

3.2 Dew formation zones – Spatial Variation of Dew Potential

3.2.1 Dew zones – a general overview

According to the cluster analysis, we identified three dew formation zones in Jordan (Figure 5). The amount of daily dew yield (i.e. mean, max (99th percentile), std) and the important climatological parameters related to dew formation (e.g., temperature, dew point temperature, and

relative humidity) are listed in Table 1. The percentiles of daily dew yield (i.e. 25th, median, 75th, and 99th percentile) are calculated in Table 1, and the 25th and 75th percentiles are illustrated in Figure 6. Eventually, the distribution of the dew formation zones in Jordan is aligned with topography, sources of moisture, and climate zones. Therefore, we named the dew zones similar to the climate zones.

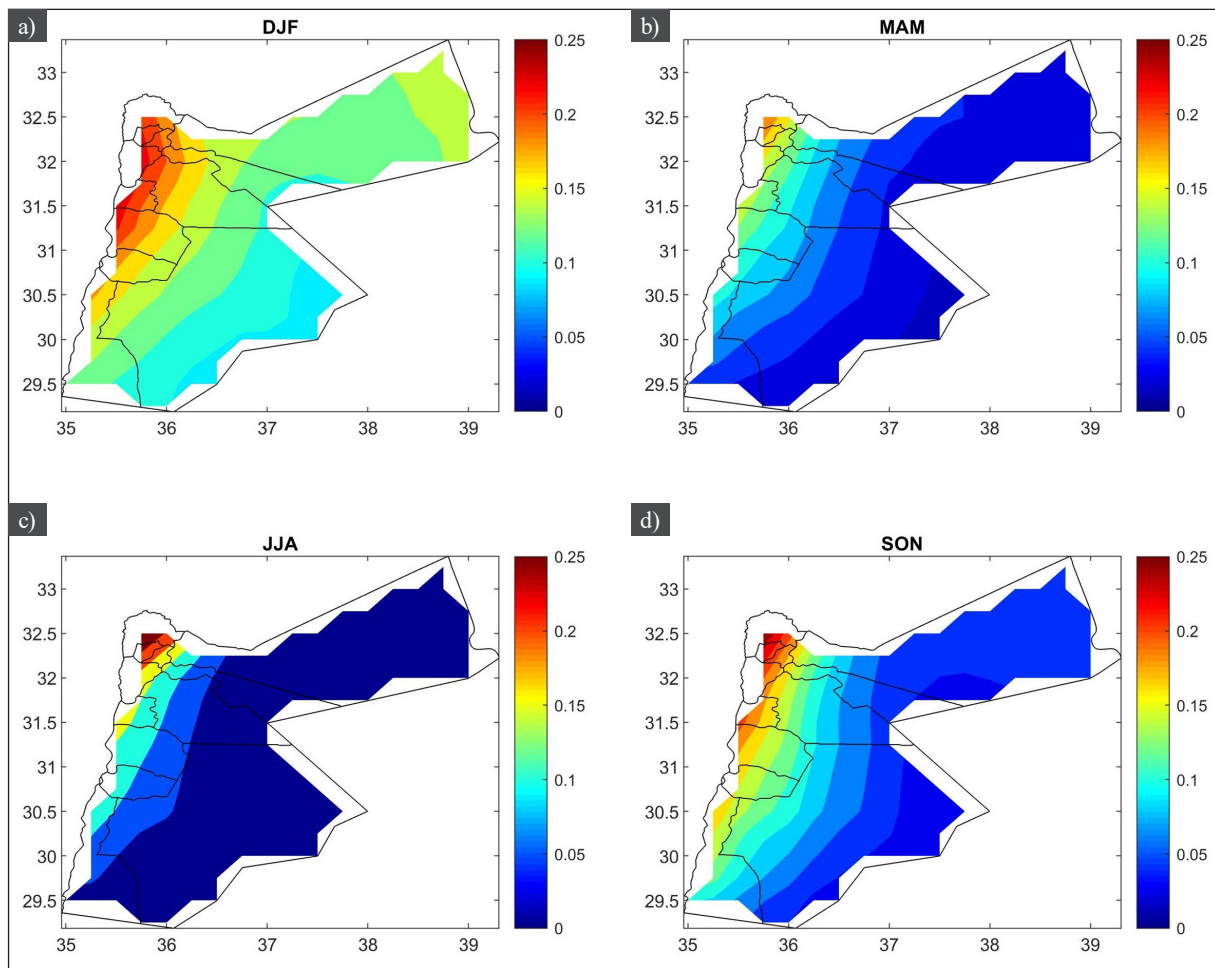


Figure 3. Cumulative dew yield [L/m²/day] presented as an overall seasonal mean during 1979–2018. (a) winter (December, January, and February), (b) spring (March, April, and May), (c) summer (June, July, and August), and (d) autumn (September, October, and November).

3.2.2 Dew zone A – Eastern desert

We identified the first dew zone (i.e. dew zone A) as the “Eastern desert”. This zone including 50% of all the grid points in Jordan is the largest dew formation. However, it has the least amount of dew occurrence and dew yields in the country. By considering the minimum harvestable dew water from the condenser (> 0.1 L/m²/day), the number of dew occurrences in this zone is about 80 days per year and the overall mean daily dew yield was $\sim 0.05 \pm 0.05$ L/m²/day, which is the lowest among other dew zones in Jordan (Figure 6 and Table 1).

The Dew period in this zone starts from October and continues through winter until the spring (namely April). However, only 80 days of this period dew can be collectible (> 0.1 L/m²/day) and for the rest of the days, the amount of dew yield is very little. From May– September dew vanished (almost Zero) in this zone (Figure 6). Indeed, this zone is characterized as the arid-hyper arid area with high temperature, no source of moisture, and low relative humidity; therefore, $T_a - T_d$ is high (about 18°C most of the time (Table 1)). Furthermore, during the warm season, high surface temperature leads to the form of thermal low-pressure systems, which cause turbulence and an intense wind speed. As such, condensation cannot occur over a long period of the year. Only during late autumn and winter due to a decrease in the temperature and domination of prevailing westerly

winds that bring the moisture from the Mediterranean Sea into the country, $T_a - T_d$ is reduced and dew can form in this zone. As such, the peak of dew yield (about 0.15 L/m²/day) is also in wintertime (December–January). The mean yearly dew yield in this zone was about 18 L/m² and the maximum was about 26 L/m² (Table 1).

3.2.3 Dew zone B – Jordan Valley

Dew zone B includes the Jordan Valley and the mountain heights plateau, which are mainly situated in the western region starting at the northern part parallel to the Jordan Valley and extending to the south approaching Wadi Rum.

Although, this zone is the smallest dew zone (including 20% of the all grid points) it has the highest potential of dew yield (overall mean daily 0.15 L/m²/day) in Jordan (Figure 6 and Table 1). Furthermore, this zone has the longest dew formation period which spans over the whole year with a significant amount of dew yield. The mean frequency of dew occurrence (> 0.1 L/m²/day) is more than 330 days/year (Figure 6 and Table 1). The mean yearly dew yield in this zone is estimated at 55 L/m² and the maximum was about 66 L/m² which is the highest in the country (Table 1). The high potential of dew formation and yield in this region is related to the fact that initial conditions for dew formation are provided during the year. For instance, this zone is located in the height mountains area so that, has a high diurnal variation of the temperature, receiving high

short-wave radiation during the day and reflecting it in the form of long-wave radiation during the night. Therefore, air temperature declines very quickly in the nighttime resulting in a reduction in $T_a - T_d$. Furthermore, this zone benefits the

efficient water bodies (e.g. Dead Sea, Mediterranean Sea, Sea of Galilee) through the westerlies or sea breeze which favors dew formation in this zone.

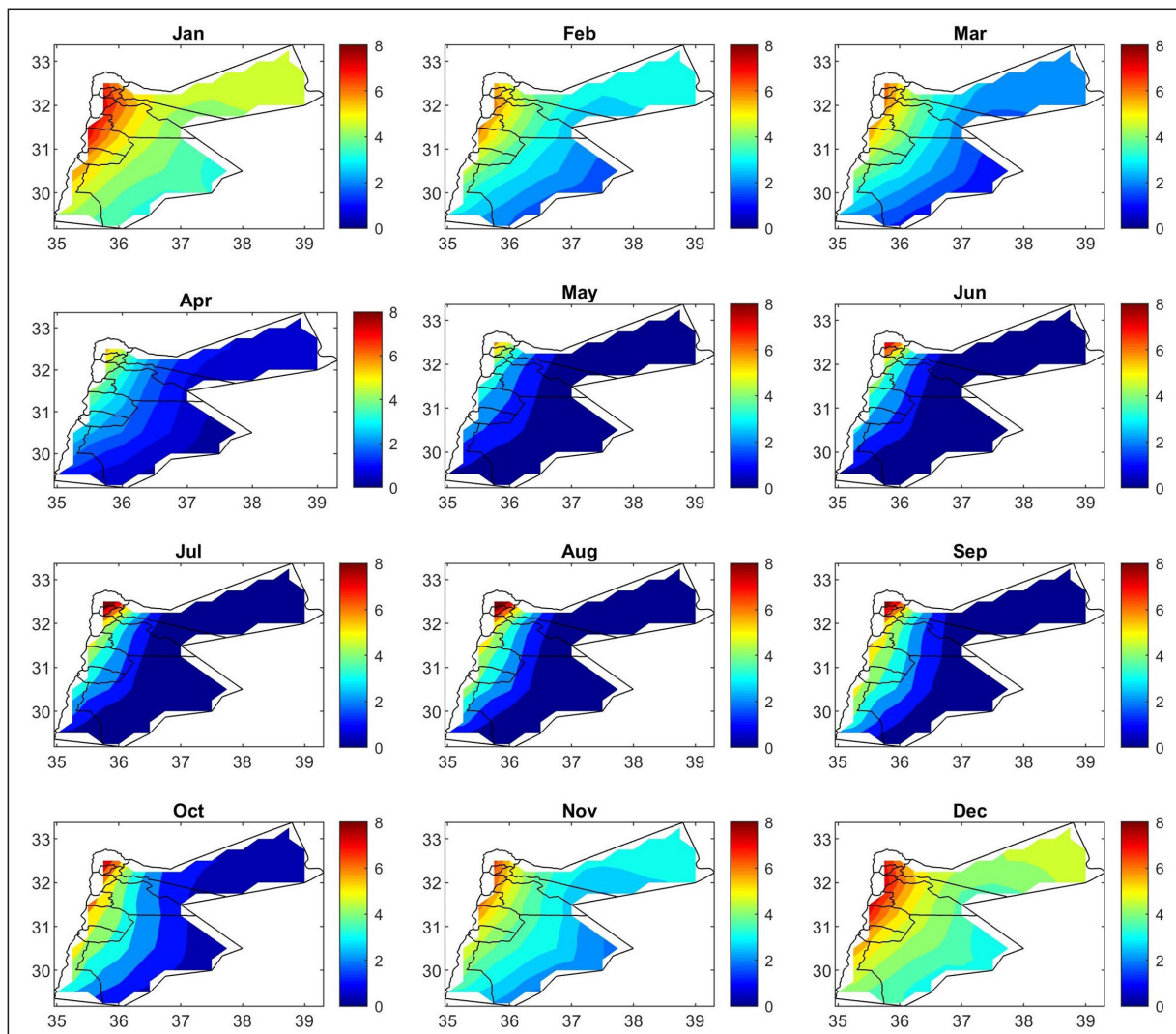


Figure 4. Cumulative dew yield [L/month] presented as an overall monthly mean during 1979–2018 in Jordan.

3.2.4 Dew zone C—Central heights Plateau

The third dew zone (dew zone C) covers the central part of Jordan from north to south including about 30% of all grid points and is geographically called East Bank Plateau. The overall mean daily dew yield in this zone is about 0.08 L/m²/day (Table 1). Although the frequency of dew occurrence in this zone is throughout the year in most cases the amount of dew is very little and negligible and the days with dew yield > 0.1 L/m² are about 120 days (Figure 6 and Table 1). The annual cycle of dew yield is clear in this zone as it was in the first dew zone with the highest yields in winter (December–January) and the lowest in late spring to late autumn (May–September). The mean yearly dew yield is about 28 L/m² and the maximum is about 36 L/m²/year (Table 1). In comparison, the potential for dew formation in this zone is more than in the first dew zone but less than in the second dew zone. However, the daily and seasonal variations are more similar to the eastern desert dew zone. Indeed, this dew zone is suffering from high temperature and low humidity,

and therefore $T_a - T_d$ rises. This condition is almost valid most of the time, only during the cold season due to a decline in temperature and increase in relative humidity dew can form on the condenser surface.

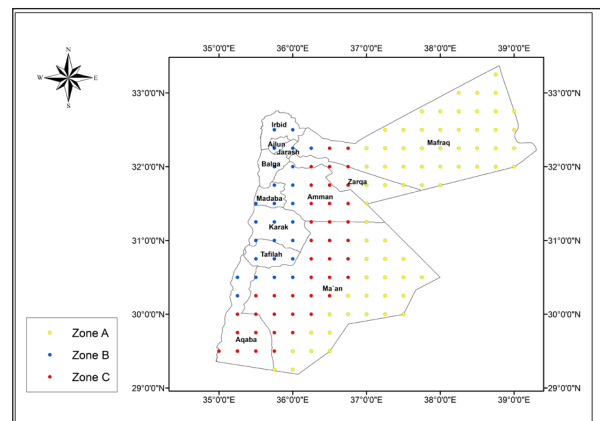


Figure 5. Dew formation zones in Jordan based on the cluster analysis of the daily cumulative dew yield during 1979–2018.

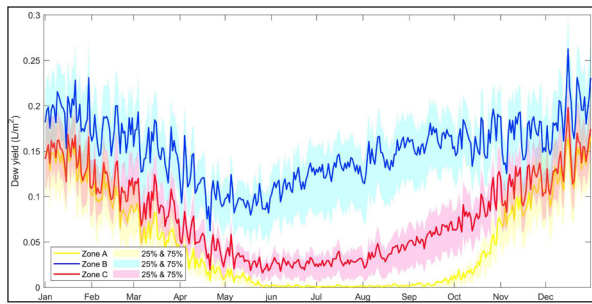


Figure 6. long-term mean seasonal variation of the cumulative daily dew yield over 40 years (1079-2018). Note that the color coding on this figure is the same and corresponds to the dew formation zones in Figure 6: (yellow) dew zone A (arid and semi-arid region), (blue) Zone B (coastal region), and (red) Zone C (central heights Plateau). The shaded parts around the lines represent the 25th and 75th percentile of daily dew yields for each cluster, and the colors are the same as clusters.

4. Discussion

Jordan is located in an arid and semi-arid region and has been suffering from fresh water scarcity over the last decades. This problem is getting even more serious with a growing population, therefore looking for a renewable source of water is vital. The atmosphere can be considered a huge reservoir of water that can be extracted in the form of dew or fog, especially in dry conditions. Based on our model simulation results to estimate the potential of dew formation in Jordan, the average dew yield was in the range of 0.05- 0.15 L/m²/ day. The outcomes are in agreement with previous observational studies that have been conducted in similar climates as Jordan (i.e. arid and semi-arid, desert, Mediterranean climates). For instance, the reported values for average daily dew yield for a semi-arid Mediterranean climate were 0.04 L/m² in Zadar (France; Muselli et al., 2009), 0.09 L/m² in Komiz'a (Croatia; Muselli et al., 2009), 0.04 L/m² in Beirut (Lebanon; Tomaszkiwicz et al., 2015), 0.06–0.19 L/m² in a semi-arid coastal area in southwestern Madagascar (Hanisch et al., 2015), and 0.13 L/m² in Beiteddine village (Lebanon; Tomaszkiwicz et al., 2017). The results are also in agreement with the desert areas in the neighboring countries, for instance, Israel (mean: 0.09 L/m²; Kidron, 1999); Dhahan, Saudi Arabia (mean: 0.22 L/m²/day; Gandhisani and Abualhamayel, 2005).

It should be noted that similar to all numerical models, this model also has some limitations that cause some uncertainties in the results, and it is expected to overestimate dew yield. However, these uncertainties caused by the model assumptions do not affect the main conclusions of this study (spatial (dew zones) and temporal variation) since it has been conducted over 40 years and averaging on a long-term smoothens the differences in daily scale.

5. Conclusions

Jordan is a country with limited water sources and comprises a wide variety of topography that defines its climate spatial variation (semi-arid, arid, and Mediterranean). It is the fourth country in the world suffering from freshwater shortages. Therefore, it is a challenging topic to find alternative sources of water for drinking and agricultural application. Dew and fog harvesting can be one of these alternative sources. However, there have been very few

investigations about dew water in Jordan. In this study, we performed gridded model simulations to estimate the dew yield during 1979–2018 aiming at investigating the spatial-temporal variation of dew formation. We also applied cluster analysis to distinguish the dew formation zones in Jordan.

Our investigation revealed that dew can occur almost everywhere in Jordan during the winter (about ~75 days during December–February). As expected, summer is the driest season with the least number of dew days in Jordan (~37 days during June–August). According to the cluster analysis, we distinguished three dew formation zones, which were closely related to the climate zones: Dew zone A (eastern desert), Dew zone B (Jordan Valley), and Dew zone C (central heights Plateau). Zone A receives the least dew formation potential, which mainly occurs during the winter, and Zone C receives the highest dew formation potential, which occurs throughout the year.

The outcomes of this study are ought to be useful for managing and planning local feasibility studies for dew harvesting and a better understanding of the feedback processes between the water cycle and climate change in Jordan.

Acknowledgment

This research was supported by the Deanship of Scientific Research at the University of Jordan, Finnish Academy (Flagship funding (grant number 337549), Center of Excellence program (CoE-ATM, grant no. 307331)), University of Isfahan is acknowledged to facilitate the research visit abroad for graduate students. Tareq Hussein acknowledges support from the Eastern Mediterranean and the Middle East—Climate and Atmosphere Research (EMME-CARE) project, which has received funding from the European Union's Horizon 2020 Research and Innovation Program (grant agreement no. 856612) and the Government of Cyprus. The European Union is not responsible for any use that may be made of the information contained therein. The sole responsibility of this publication lies with the author.

References

- Abdulla, F. 21st Century Climate Change Projections of Precipitation and Temperature in Jordan. 1st International Conference on Optimization-Driven Architectural Design (OPTARCH 2019). *Proced. Manuf.* 2020, 44, 197–204.
- Al-Shuaibi R. (2021) Investigation of Dew Water Harvesting Quantity and Quality at Selected Sites in Jordan. Master Thesis, Faculty of Science, Department of Geology, The University of Jordan. Unpublished M.Sc. Thesis.
- Atashi, N.; Rahimi, D.; Al Kuisi, M.; Jiries, A.; Vuollekoski, H.; Kulmala, M.; Vesala, T.; Hussein, T. "Modeling Long-Term Temporal Variation of Dew Formation in Jordan and Its Link to Climate Change." *Water*, 2020, 12, 21–86.
- Beysens, D. Dew nucleation, and growth. *C. R. Phys.* 2006, 7, 1082–1100.
- Beysens, D. Estimating dew yield worldwide from a few meteo data. *Atmos. Res.* 2016, 167, 146–155.
- Beysens, D. The formation of dew. *Atmos. Res.* 1995, 39, 215–237.
- Beysens, D.; Clus, O.; Mileta, M.; Milimouk, I.; Muselli, M.; Nikolayev, VS. Collecting dew as a water source on small islands: The dew equipment for water project in (Croatia).

- Energy 2007, 32, 1032–1037.
- Beysens, D.; Milimouk, I.; Nikolayev, V.; Muselli, M.; Marcillat, J. Using radiative cooling to condense atmospheric vapor: A study to improve water yield. *J. Hydrol.* 2003, 276, 111.
- Beysens, D.; Muselli, M.; Milimouk, I.; Ohayone, C.; Berkowicz, S.M.; Soyeuxg, E.; Mileta, M.; Ortega, P. Application of passive radiative cooling for dew condensation. *Energy* 2006a, 31, 1967–1979.
- Beysens, D.; Muselli, M.; Nikolayev, V.; Narhe, R.; Milimouk, I. Measurement, and modelling of dew in island, coastal and alpine areas. *Atmos. Res.* 2005, 73, 122.
- Beysens, D.; Ohayon, C.; Muselli, M.; Clus, O. Chemical and biological characteristics of dew and rainwater in an urban coastal area (Bordeaux, France). *Atmos. Environ.* 2006b, 40, 3710–3723.
- Berrisford, P.; Dee, D.; Poli, P.; Brugge, R.; Fielding, K.; Fuentes, M.; Kallberg, P.; Kobayashi S.; Uppala, S.; Simmons, A. ERA report series, The ERA-Interim archive, version 2, Shinfield Park, Reading, available at: <https://www.ecmwf.int/en/elibrary/8174-era-interim-archive-version-20> (last access: 7 August 2021), 2011.
- Bunkers, M. J.; Miller Jr, J. R. Definition of climate regions in the Northern Plains using an objective cluster modification technique. *J. Climate*, 1996, 9, 130–146, [https://doi.org/10.1175/1520-0442\(1996\)009<0130:DOCRIT>2.0.CO;2](https://doi.org/10.1175/1520-0442(1996)009<0130:DOCRIT>2.0.CO;2).
- Clus, O.; Ortega, P.; Muselli, M.; Milimouk, I.; Beysens, D. Study of dew water collection in humid tropical islands. *J. Hydrol.* 2008, 361, 159–171.
- Dee, D. P.; Uppala, S. M.; Simmons, A. J.; Berrisford, P.; Poli, P.; Kobayashi, S.; Andrae, U.; Balmaseda, M. A.; Balsamo, G.; Bauer, P.; Bechtold, P.; Beljaars, A. C. M.; van de Berg, L.; Bidlot, J.; Bormann, N.; Delsol, C.; Dragani, R.; Fuentes, M.; Geer, A. J.; Haimberger, L.; Healy, S. B.; Hersbach, H.; Hólm, E. V.; Isaksen, I.; Kållberg, P.; Köhler, M.; Matricardi, M.; McNally, A. P.; Monge-Sanz, B. M.; Morcrette, J.-J.; Park, B.-K.; Peubey, C.; de Rosnay, P.; Tavalato, C.; Thépaut, J.-N.; and Vitart, F. The ERA-Interim reanalysis: configuration and performance of the data assimilation system. *Q. J. Roy. Meteorol. Soc.* 2011, 137, 553–597. <https://doi.org/10.1002/qj.828>.
- Freiwan, M.; Kadioglu, M. Climate variability in Jordan. *Int. J. Climatol.* 2008, 28, 69–89.
- Galek, G.; Sobik, M.; Blas, M.; Polkowska, Z.; Cichala-Kamrowska, K. Dew formation and chemistry near a motorway in Poland. *Pure Appl. Geophys.* 2012, 169, 1053–1066.
- Galek, G.; Sobik, M.; Błaś, M.; Polkowska, Z.; Cichala-Kamrowska, K.; Wałaszek, K. Dew and hoarfrost frequency, formation efficiency and chemistry in Wrocław, Poland. *Atmos. Res.* 2015, 151, 120–129.
- Gandhisani, P.; Abualhamayel, H.I. Modelling and testing of a dew collection system. *Desalination* 2005, 18, 47–51.
- Hadadin, N. Dams in Jordan current and future perspective. *Can. J. Pure Appl. Sci.* 2015, 9, 3279–3290.
- Hamdy, A.; Lacirignola, C. Mediterranean water resources: Major challenges towards the 21st century. In *Proceedings of the International Seminar on Mediterranean Water Resources: Major Challenges Towards the 21st Century*, Egypt, Cairo, 1–5 March 1999.
- Hamed, A.M.; Kabeel, A.E.; Zeidan, E.S.B.; Aly, A.A. A technical review on the extraction of water from atmospheric air in arid zones. *Int. J. Heat Mass Trans.* 2010, 4, 213–228.
- Hanisch, S.; Lohrey, C.; Buerkert, A. Dewfall, and its ecological significance in semi-arid coastal southwestern Madagascar. *J. Arid. Environ.* 2015, 121, 24–31, <https://doi.org/10.1016/j.jaridenv.2015.05.007>.
- Jacobs, A.F.G.; Heusinkveld, B.G.; Berkowicz, S.M. Passive dew collection in a grassland area, The Netherlands. *Atmos. Res.* 2008, 87, 377–385.
- Jiries, A. Chemical composition of dew in Amman, Jordan. *Atmos. Res.* 2001, 57, 261–268.
- Jorge Ernesto, A.T.; Jose Jasson, F.P. Winter dew harvest in Mexico City. *Atmosphere* 2016, 7, 2.
- Jumikis, A.R. Aerial wells: Secondary source of water. *Soil Sci.* 1965, 100, 83–95.
- Khalil, B.; Adamowski, J.; Shabbir, A.; Jang, C.; Rojas, M.; Reilly, K.; OzgaZielinski, B. A review: Dew water collection from radiative passive collectors to recent developments of active collectors. *Sustain. Water Resource. Manag.* 2016, 2, 71–86.
- Kidron, G. J. Altitude dependent dew and fog in the Negev Desert, Israel. *Agr. Forest. Meteorol.* 1999, 96, 1–8, [https://doi.org/10.1016/S0168-1923\(99\)00043-X](https://doi.org/10.1016/S0168-1923(99)00043-X).
- Kidron, G.J.; Herrnstadt, I.; Barzilay, E. The role of dew as a moisture source for sand microbiotic crusts in the Negev Desert, Israel. *J. Arid Environ.* 2002, 52, 517–533.
- Lekouch, I.; Mileta, M.; Muselli, M.; Milimouk-Melnitochouk, I.; Šojat, V.; Kabbachi, B.; Beysens, D. Comparative chemical analysis of dew and rainwater. *Atmos. Res.* 2010, 95, 224–234.
- Lekouch, I.; Muselli, M.; Kabbachi, B.; Ouazzani, J.; MelnitochoukMilimouk, I.; Beysens, D. Dew, fog, and rain as supplementary sources of water in southwestern Morocco. *Energy* 2011, 36, 2257–2265.
- Lindblom, J.; Nordell, B. Water production by underground condensation of humid air. *Desalination* 2006, 189, 248–260.
- MaestreValero, J.F.; MartínezAlvarez, V.; Baille, A.; MartínGórriz, B.; GallegoElvira, B. Comparative analysis of two polyethylene foil materials for dew harvesting in a semiarid climate. *J. Hydrol.* 2011, 410, 84–91.
- Mileta, M.; Beysens, D.; Nikolayev, V.; Milimouk, I.; Clus, O.; Muselli, M. Fog, and Dew Collection Projects in Croatia. Available online: <https://arxiv.org/ftp/arxiv/papers/0707/0707.2931.pdf>. (accessed on 22 November 2019).
- Monteith, J.L. Dew. *Q. J. R. Meteorol. Soc.* 1957, 83, 322–341.
- Muselli, M.; Beysens, D.; Marcillat, J.; Milimouk, I.; Nilsson, T.; Louche, A. Dew water collector for potable water in Ajaccio (Corsica Island, France). *Atmos. Res.* 2002, 64, 297–312.
- Muselli, M.; Beysens, D.; Mileta, M.; Milimouk, I. Dew and rainwater collection in the Dalmatian Coast, Croatia. *Atmos. Res.* 2009, 92, 455–463.
- Nielsen, F. Introduction to HPC with MPI for Data Science, in: chap. 8: Hierarchical Clustering, Springer, Switzerland, 2016.
- Nikolayev, V.S.; Beysens, D.; Gioda, A.; Milimouka, I.; Katiushin, E.; Morel, J.P. Water recovery from dew. *J. Hydrol.* 1996, 182, 19–35.
- Nikolayev, V.S.; Beysens, D.; Muselli, M. A computer model for assessing dew/frost surface deposition. In *Proceedings of the Second International Conference on Fog and Fog Collection*, St John's, NL, Canada, 15–20 July 2001; pp. 333–336.
- Nilsson, T. Initial experiments on dew collection in Sweden and Tanzania. *Sol. Energy Mater. Sol. Cells* 1996, 40, 23–32.
- Nilsson, T.M.J.; Vargas, W.E.; Niklasson, G.A.; Granqvist, C.G. Condensation of water by radiative cooling. *Ren. Energy* 1994, 5, 310–317.
- Odeh, I.; Arar, S.; Al-Hunaiti, A.; Sa'aydeh, H.; Hammad, G.; Duplissy, J.; Vuollekoski, H.; Korpela, A.; Petäjä, T.; Kulmala, M.; et al. Chemical investigation and quality of urban dew collection with dust precipitation. *Environ. Sci. Pollut. Res.* 2017, 24, 12312–12318.

- Pedro, M.J., Jr.; Gillespie, T.J. Estimating dew duration. I. Utilizing micrometeorological data. *Agric. Meteorol.* 1981, 25, 283–296.
- Polkowska, Ż.; Błaś, M.; Klimaszewska, K.; Sobik, M.; Małek, S.; Namieśnik, J. Chemical characterization of dew water collected in different geographic regions of Poland. *Sensors* 2008, 8, 4006–4032.
- Rajvanshi, A.K. Large scale dew collection as a source of fresh water supply. *Desalination* 1981, 36, 299–306.
- Raman, C.R.V.; Venkatraman, S.; Krishnamurthy, V. Dew over India and Its Contribution to Winter-Crop Water Balance. *Agric. For. Meteorol.* 1973, 11, 17–35.
- Richards, K. Observation and simulation of dew in rural and urban environments. *Prog. Phys. Geogr.* 2004, 28, 76–94.
- Sharan, G. Dew Yield from Passive Condensers in a Coastal Arid Area: Kutch. Available online: <http://vslir.iima.ac.in:8080/jspui/bitstream/11718/6362/1/2005-01-05gsharan.pdf>. (accessed on 22 November 2019).
- Sharan, G.; Shah, R.; Millimouk-Melnythouk, I.; Beysens, D. Roofs as Dew Collectors: Corrugated Galvanized Iron Roofs in Kothara and Suthari (NW India). In *Proceedings of the Fourth International Conference on Fog, Fog Collection and Dew, La Serena, Chile, 22–27 July 2007*.
- Tomaszkiewicz, M.; Abou Najm, M.; Beysens, D.; Alameddine, I.; El-Fadel, M. Dew as a sustainable non-conventional water resource: A critical review. *Environ. Rev.* 2015, 23, 425–442.
- Tomaszkiewicz, M.; Abou Najm, M.; Beysens, D.; Alameddine, I.; Zeid, E.B.; El-Fadel, M. Projected climate change impacts upon dew yield in the Mediterranean basin. *Sci. Total Environ.* 2016, 566, 1339–1348.
- Tomaszkiewicz, M.; Abou Najm, M.; Zurayk, R.; El-Fadel, M. Dew as an adaptation measure to meet water demand in agriculture and reforestation, *Agr. Forest. Meteorol.* 2017, 232, 411–421, <https://doi.org/10.1016/j.agrformet.2016.09.009>.
- Vuollekoski, H.; Vogt, M.; Sinclair, V.A.; Duplissy, J.; Järvinen, H.; Kyrö, E.; Makkonen, R.; Petäjä, T.; Prisle, N.L.; Räisänen, P.; et al. Estimates of global dew collection potential on artificial surfaces. *Hydrol. Earth Syst. Sci.* 2015, 19, 601–613.
- Ye, Y.; Zhou, K.; Song, L.; Jin, J.; Peng, S. Dew amount and its correlation with meteorological factors in urban landscapes of Guangzhou, China. *Atmos. Res.* 2007, 86, 21–29.
- Yim, O.; Ramdeen, K. T. Hierarchical cluster analysis: comparison of three linkage measures and application to psychological data, *Quant. Meth. Psychol.* 2015, 11, 8–21, <https://doi.org/10.20982/tqmp.11.1.p008>.

Appendix: “Supplementary Material”

Long-Term Model Simulation and a Spatial-Temporal Investigation for Dew Potential in Jordan

Nahid Atashi and Tareq Hussein

S.1. Model Description

The model describes the water phase change based on mass and heat balance Equation

$$\frac{dT_c}{dt} (C_c m_c + C_w m_w + C_i m_i) = P_{rad} + P_{cond} + P_{conv} + P_{lat} \dots \quad (S1)$$

where dT_c/dt is the change rate in the condenser temperature. C_c , C_w , and C_i are the specific heat capacity of condenser, water, and ice; respectively. Here, m_c , m_w , and m_i are mass of condenser, water, and ice; respectively. The right-hand side describes the heat exchange involved in the heat exchange processes: P_{rad} is the incoming and outgoing radiation, P_{cond} is the conductive heat exchange between the condenser surface and the ground, P_{conv} is the convective heat exchange, and P_{lat} is the latent heat released by the condensation or desublimation of water. The model reads all input data for a given grid point and solves equations. using a fourth-order Runge–Kutta algorithm with a 10 s time step. All terms in Equation (S1) are described in more detail in Tables S1 and S2.

The model was set up so that it assumes similar conditions for the phase-change of pre-existing water or ice on the condenser sheet. For instance, if the water on the condenser is in the liquid phase (i.e., $m_w > 0$) and the condenser temperature $T_c < 0$ °C, then the sheet is losing energy (i.e., the right-hand side of Equation (S1) is negative). In that case, instead of solving Equation (S1), T_c is assumed constant and the lost mass from the liquid phase of water is transferred to the cumulated mass of ice; i.e., the water is transformed from liquid phase to solid phase. Consequently, Equation (S1) is replaced by

$$L_{wi} \frac{dm_w}{dt} = P_{rad} + P_{conv} + P_{lat}, \dots \quad (S2)$$

where L_{wi} [J kg⁻¹] is the latent heat of fusion. If the water

on the condenser is in the solid phase (i.e., $m_i > 0$) and the condenser temperature $T_c > 0$ °C, a similar equation is assumed for the change rate of ice mass (m_i).

Note that Equation (S2) is not related to the condensation of water; it only describes the phase change of the already condensed water or ice on the condenser. For the water condensation rate, which is assumed independent of Equation (S2), the mass-balance equation is then assumed to be

$$\frac{dm}{dt} = \max [0, S_c k (P_{sat}(T_d) - P_c(T_c))], \dots \quad (S3)$$

where m represents either the mass of ice (m_i) or water (m_w) depending on whether T_c is below or above 0 °C. $P_{sat}(T_d)$ is the saturation pressure at the dew point temperature whereas $P_c(T_c)$ is the vapor pressure over the condenser sheet. $k = h / L_{vw} \gamma = 0.622h / C_a p$ is the mass transfer coefficient, where L_{vw} [J kg⁻¹] is the specific latent heat of water vaporization, γ is the psychrometric constant, C_a is the specific heat capacity of air, and p is the atmospheric air pressure. Here, $h = 5.9 + 4.1 u (511 + 294) / (511 + T_a)$ is the heat transfer coefficient, where u and T_a are the prevailing horizontal wind speed and the ambient temperature at 2 m from the ground.

In practice, the wettability of the surface affects vapor pressure P_c directly above it. In other words, P_c is lower over a wet surface; thus, condensation may take place even if $T_c > T_d$ (e.g., [15]). According to the model setup, Equation (S3) assumes irreversible condensation; i.e., there is no evaporation or sublimation during daytime even if $T_c > T_a$. Furthermore, the model simulation resets the cumulative values for water and ice condensation at noon. and takes the preceding maximum value of $m_w + m_i$ as the representative daily yield. This way, the model simulation replicates the daily manual dew water collection of the condensed water around sunrise; i.e., after which T_c is often above the dew point temperature.

Table S1. Description of the dew formation model by listing the terms in Equation (S1).

Term	Unit	Description
dT_c/dt	$K s^{-1}$	The change rate of the condenser temperature
T_c	K	The temperature of the condenser
T	s	Time. Here the time step in the model was 10 s
C_c	$J kg^{-1} K^{-1}$	Specific heat capacity of the condenser. For low-density polyethylene (LDPE) and polymethylmethacrylate (PMMA) it is $2300 J kg^{-1} k^{-1}$
C_i	$J kg^{-1} K^{-1}$	Specific heat capacity of ice ($2110 J kg^{-1} k^{-1}$)
C_w	$J kg^{-1} K^{-1}$	Specific heat capacity of water ($4181.3 J kg^{-1} k^{-1}$)
m_c	kg	Mass of the condenser given by $m_c = \rho_c S_c \delta_c$ where ρ_c , S_c , and δ_c are the density (here it is $920 kg m^{-3}$), surface area (here it is $1 m^2$), and thickness of the condenser (here it is $0.39 mm$)
m_i	kg	Mass of ice
m_w	kg	Mass of water, representing the cumulative mass of water that has
P_{rad}	W	Heat exchange due to incoming and outgoing radiation $P_{rad} = (1 - a) S_c R_{sw} + \varepsilon_c S_c R_{lw} - S_c \varepsilon_c \sigma T_c^4$ where a is the condenser short-wave albedo (here it is 0.84), S_c is the condenser surface area (here it is $1 m^2$), ε_c is the emissivity of the condenser (here it is 0.94), σ is Stephan-Boltzmann constant ($5.67 \times 10^{-8} W m^{-2} K^{-4}$), T_c [K] is the temperature of the condenser, and R_{sw} and R_{lw} [$W m^{-2}$] are the incoming short-wave radiation (i.e., surface solar radiation downwards) and incoming long-wave radiation (i.e., surface thermal radiation downwards)
P_{cond}	W	Conductive heat exchange between the condenser surface and the ground. For simplicity, we assumed that the condenser is perfectly insulated from the ground; i.e., $P_{cond} = 0$
P_{conv}	W	Convective heat exchange $P_{conv} = S_c (T_a - T_c) h$ where S_c is the condenser surface area (here it is $1 m^2$), T_a [K] is the ambient temperature at 2 m from the ground, T_c [K] is the temperature of the condenser, and h [$W m^{-2} K^{-1}$] is the heat transfer coefficient that is estimated based on a semi-empirical equation [37] $h = 5.9 + 4.1 WS (511 + 294)/(511 + T_a)$ and here WS [$m s^{-1}$] is the prevailing horizontal wind speed at 2 m from the ground.
P_{lat}	W	Latent heat released by the condensation or desublimation of water $P_{lat} = \begin{cases} L_{vw} \frac{dm_w}{dt} & T_c > 0^\circ C \\ L_{vi} \frac{dm_i}{dt} & T_c < 0^\circ C \end{cases}$ where L_{vw} [$J kg^{-1}$] is the specific latent heat of water vaporization and L_{vi} [$J kg^{-1}$] is specific latent heat of water desublimation. Here, dm_w/dt is the change rate of water whereas dm_i/dt is the change rate of ice

Table S2. A list of nomenclature.

Parameter	Unit	Description
α		Albedo of the condenser sheet
C_a	$J\ kg^{-1}\ K^{-1}$	Specific heat capacity of air
C_c	$J\ kg^{-1}\ K^{-1}$	Specific heat capacity of the condenser
C_i	$J\ kg^{-1}\ K^{-1}$	Specific heat capacity of ice
C_w	$J\ kg^{-1}\ K^{-1}$	Specific heat capacity of water
DP	K	Dew point temperature
h	$W\ K^{-1}\ m^{-2}$	Heat transfer coefficient
k	Per s^{-1}	Mass transfer coefficient
L_{vi}	$J\ kg^{-1}$	Specific latent heat of desublimation for water
L_{vw}	$J\ kg^{-1}$	Specific latent heat of vaporization for water
L_{wi}	$J\ kg^{-1}$	Latent heat of fusion
m_c	kg	Mass of the condenser
m_i	kg	Mass of ice
m_w	kg	Mass of water
p	Pa	Atmospheric air pressure
p_c	Pa	Vapour pressure over condenser
p_{sat}	Pa	Saturation pressure of water
P_{cond}	W	Conductive heat exchange between the condenser surface and the ground
P_{conv}	W	Convective heat exchange
P_{lat}	W	Latent heat released by the condensation or desublimation of water
P_{rad}	W	Heat exchange due to incoming and outgoing radiation
R_{lw}	$W\ m^2$	Surface thermal radiation downwards
R_{sw}	$W\ m^2$	Surface solar radiation downwards
S_c	m^2	Surface area of condenser
T_a	K	Ambient temperature at 2 m
T_c	K	The temperature of the condenser
U_{10}	$m\ s^{-1}$	Horizontal wind speed component at 10 m
V_{10}	$m\ s^{-1}$	Horizontal wind speed component at 10 m
WS	$m\ s^{-1}$	Prevailing horizontal wind speed at 2 m
z_0	m	Surface roughness
c	mm	Condenser sheet thickness
ϵ		Emissivity of condenser sheet
	$Pa\ K^{-1}$	Psychrometric constant
	$W\ m^{-2}\ k^{-4}$	Stefan–Boltzmann constant

S2. Cluster analysis

We used hierarchical agglomerative clustering which consists of four main steps:

1. calculating the distance measured between all entries (data points);
2. merging the two closest entries as a new cluster;
3. recalculating the distance between all entries;
4. repeat steps 2 and 3 until all entries are grouped into distinct groups (i.e., clusters).

Similarity measurement is a critical step in the hierarchical approach which influences the shape of the clusters [62]. The “Euclidean distance” is the most common distance metric and is widely used in atmospheric science. The Euclidean distance between two objects i and j in a two-dimensional data matrix X (here the number of rows represented the number of spatial grid points in the model simulation domain and the number of columns represented the cumulative daily dew yield) is simply the squared

difference between them for each of p variables, summed over the variables and k is the number of clusters [63]. This can be written as

$$d_{ij} = \sqrt{\sum_{k=1}^p (x_{ik} - x_{jk})^2}$$

The next step is merging the two closest entries (grid points) to form a new cluster based on a linkage criterion. There are some commonly used linkage criteria: single linkage, complete linkage, average distance, and Ward’s minimum variance methods, which differ in how the distances between entries are calculated and how the two closest entries are defined [64]. Here, we used Ward’s method for further analysis [65], which is the most frequent clustering technique used in climate research and it gives the most consistent clusters [61,66–68]. It calculates the means of all variables (the amount of dew) within each cluster, then calculates the Euclidean distance to the cluster mean of each

case, and finally sums across all grid points [69]. In any CA, the optimal number of clusters is an important issue; however, there is no reliable and universally accepted method to decide the number of clusters and it can be a limitation when using CA, because the number of clusters also determines the amount of variance in each group. Therefore, the number of

clusters should be selected so that both the number of groups and the variance within the groups are minimal. There are a few suggestions about the optimum number of clusters [69–71]. Although, this information can be used as an indicator to decide the number of clusters a visual check of the result can still help to make the right decision.